ISSN 2277-3061

Binary Quantum Communication using Squeezed Light: Numerical, Simulation, and Experimental Results

Ismael S. Desher Alaskary[1] and R. S. Fyath[2]

[1]Institute of Laser for Postgraduate Studies, University of Baghdad, Baghdad, Iraq

Desher19@yahoo.com

[2]College of Engineering, Alnahrain University, Baghdad, Iraq

rsfyath@yahoo.com

ABSTRACT

In this paper, the squeezed quantum state is generated using an optical parametric oscillator via a spontaneous parametric down conversion technique to investigate squeezed states with quantum noise in one quadrature below the standard quantum limit at the expense of the other. The setup involves four main parts: generation of Nd-YAG second harmonic via a ring resonator, squeezed cavity with a nonlinear crystal inside to generate the squeezed state, Pound-Drever-Hall technique to stabilize the laser in the squeezed cavity and balanced homodyne receiver with high efficiency to detect the squeezed state. A comparison in error probability is addressed between the quantum coherent classical and the quantum squeezed non-classical state in the presence of thermal noise and the dissipation. It is found that with extremely low number of photons, the squeezed state is robust against channel noise.

Indexing terms/Keywords

Squeezed light; Quantum binary communication.

Academic Discipline And Sub-Disciplines

Quantum communication.

SUBJECT CLASSIFICATION

90C26.

TYPE (METHOD/APPROACH)

Theoretical, simulation, and experimental investigation.

ISSN 2277-3061

1 SIMULATION WORK

This section simulates the generation of squeezed state and its application in binary quantum communication. The error probability is theoretically computed and compared with the error probability of the simulation results. The simulation work is based on MATLAB R2012a, MATHCAD 15, KaleidaGraph, and LABVIEW. The program involves three parts: transmitter, channel, and receiver.

(i) The transmitter

The sender generates randomly two real coherent states $-|\alpha\rangle$ and $|\alpha\rangle$, encoded in two digits 0 and 1, respectively, and then transmits the state to the receiver through a noisy channel with the following parameters at time $t = 0$

1. The average number of photons

$N_{coh,0} = \alpha^2$

2. The variance

$(\Delta q_{coh,0})^2 = (\Delta p_{coh,0})^2 = \frac{1}{2}$

(ii) The channel

The signal during transmission is affected by the following parameters

1. The thermal noise from the environment represented by the thermal photons number N_{th} which is taken as a varying parameter during simulation.
2. The attenuation represented by $G = \exp(-\Gamma t)$. Note that when t varies from 0 to ∞, G varies from 1 to 0.

(iii) The receiver

The state after time t becomes noisy and has a new parameters

1. The average number of photons

$N_{coh,t} = G\alpha^2$

2. The variance

$(\Delta q_{coh,t})^2 = (\Delta p_{coh,t})^2 = \frac{1}{2}G + (1-G)\frac{1}{2}(1+2N_{th})$

Note that the last equation has a physical meaning when $t = 0$. Here $G = 1$ and the variance equals to 1/2. Therefore, it specifies the initial coherent state. When t approaches ∞, $G = 0$ thus the coherent state is evolved to the thermal state after infinite time.

Binary phase shift keying (PSK) digital modulation is usually used in binary quantum communication in order to modulate the quantum states So two coherent states $|\alpha_1\rangle = |\alpha\rangle$ and $|\alpha_2\rangle = -|\alpha\rangle$ are encoded in 0 and 1, respectively, then transmitted through a noisy channel. These two signals, in the absence of all noise, are separated in the phase-space representation by 2α where α is a real amplitude. The average number of photons is given by $N = |\alpha|^2$. In addition, these coherent states are not orthogonal therefore; a correlation between them will be occurred. In order to compute the probability of error, the receiver needs to take a decision to distinguish whether the incoming state is $-|\alpha\rangle$ or $|\alpha\rangle$. The two signals are received by homodyne detection, which provides the advantage of amplifying the weak signal by mixing it with a strong local oscillator (LO) field.

Starting with the squeezed vacuum state at t=0, squeezed vacuum state is a Gaussian state with average mean number of photons N_{sq} and two different variances according to the phase quadrature

$$N_{sq,0} = \sinh^2(r) \quad (1)$$

$$\begin{cases} (\Delta q_{sq,0})^2 = \frac{1}{2}\exp(-2r) \\ (\Delta p_{sq,0})^2 = \frac{1}{2}\exp(2r) \end{cases} \quad (2)$$

where r is the squeezed parameter and $(\Delta q_{sq})^2$, $(\Delta p_{sq})^2$ are the squeezing and anti-squeezing variances, respectively.

Next, after time t the state evolves during transmission and will be exposed by environment represented by N_{th} and dissipation G. Thus, the average number of photons and the variance can be expressed as

$$N_{sq,t} = [\alpha^2 + \sinh^2(r)]G \quad (3)$$

$$\begin{cases} (\Delta q_{sq,t})^2 = G(\Delta q_{sq,0})^2 + (1-G)\left(\frac{1}{2} + N_{th}\right) \\ (\Delta p_{sp,t})^2 = G(\Delta p_{sp,0})^2 + (1-G)\left(\frac{1}{2} + N_{th}\right) \end{cases} \quad (4)$$

Now, adding $\pm(1/2)\exp(-2r)$ to Eqn. (4) then arranging the expression to get

$$\begin{cases} (\Delta q_{sq,t})^2 = (\Delta q_{sq,0})^2 + (1-G)\left\{\frac{1}{2}[1-\exp(-2r)] + N_{th}\right\} \\ (\Delta p_{sp,t})^2 = (\Delta p_{sp,0})^2 + (1-G)\left\{\frac{1}{2}[1-\exp(2r)] + N_{th}\right\} \end{cases} \quad (5)$$

Eqn. (5) represents the variance of the evolved state in time t. Thus, the state at the detection can be fully represented by the density matrix operator ρ_{sq} which is a convolution of the thermal state with the squeezed coherent state

$$\rho_{sq} = \iint \frac{\exp[-(x^2+y^2)/2\Sigma^2]}{2\pi\Sigma^2} |r,\emptyset\rangle\langle r,\emptyset| dr d\emptyset \quad (6)$$

where Σ^2 is the variance of the thermal state which can be written as

$$\Sigma^2 = \frac{1}{2}(1-G)\left\{\frac{1}{2}[1-\exp(-2r)] + N_{th}\right\} \quad (7)$$

Therefore, the generated state is a squeezed coherent state $|\alpha_{sq}\rangle$ affected by N_{th} and dissipation G

$$|\alpha_{sq}\rangle = |a_{sq}\, exp(-i\varphi_{sq})\rangle = |r\, exp(i\emptyset) \pm \sqrt{G}\sqrt{\alpha^2 + \sinh^2(r)}\rangle \quad (8)$$

where a_{sq} and φ_{sq} are the amplitude and the phase of the transmitted state respectively. Hence these parameters can be expressed as

$$\begin{cases} a_{sq} = \sqrt{r^2 + G[\alpha^2 + \sinh^2(r)] + 2\sqrt{G}\sqrt{\alpha^2 + \sinh^2(r)}\, cos\emptyset} \\ \varphi_{sq} = arctan\left[\frac{r sin\emptyset}{a_{sq} + r cos\emptyset + \sqrt{G}\sqrt{\alpha^2 + \sinh^2(r)}}\right] \end{cases} \quad (9)$$

where α_{sq} is real and the angle φ_{sq} is between –π and π.

1.1 Generation of Squeezed Vacuum State

The squeezed vacuum state is different from the vacuum state in the sense of the number of photons because the last has no photons while the first has a number of photons equals to $sinh(r)$ as shown in Figure 1. The squeezed parameter r is fixed at 0.8 in all the following results.

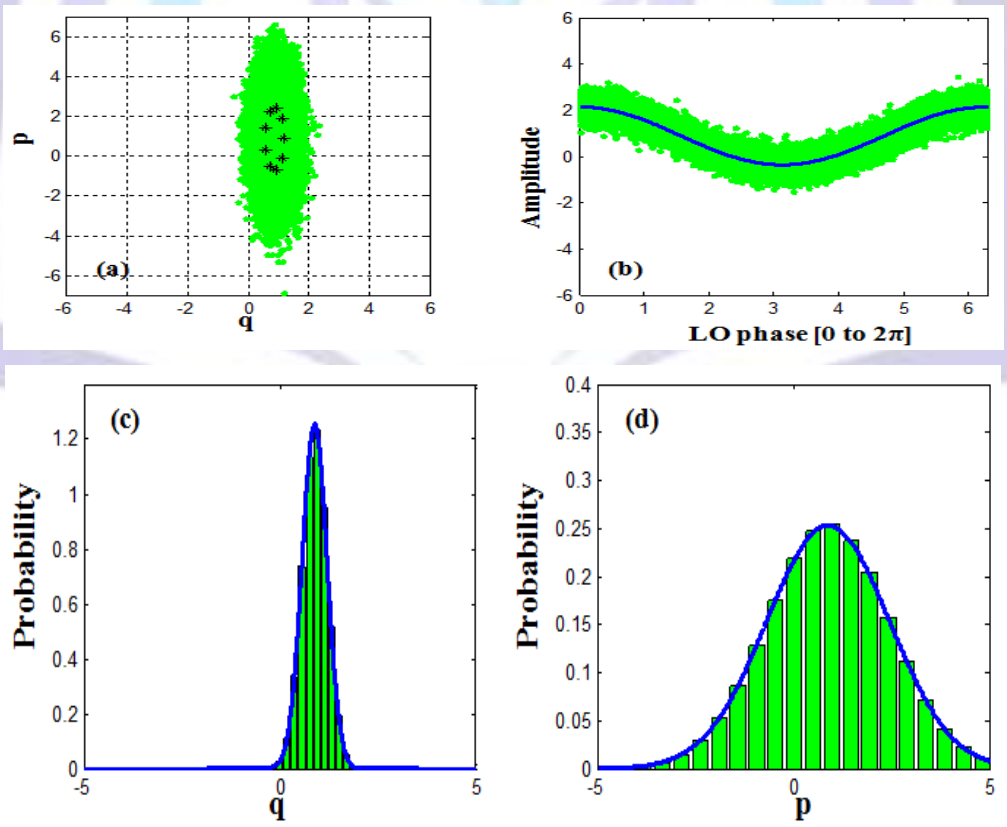

Figure 1: Squeezed vacuum state. Simulation results for $\alpha^2 = 0$, N_{th}=0 and G=1. (a) Phase-space representation. (b) Amplitude scan. (c) Probability distribution of the amplitude. (d) Probability distribution of the phase. The blue curve is the fitted Gaussian shape.

In Figure 1a, the squeezed state is not centered. It is tilted by $sinh(r)$. In addition, the trace of the homodyne detection in Figure 1b is a strong indication to the number of photons because the fitted curve is a sine wave. Lastly, Figures 1c and 1d show the histograms of the marginal probability of the squeezed amplitude and the stretched phase, respectively. They have Gaussian distribution with 0.89 mean and standard deviation of 0.32 and 1.57, respectively.

1.2 Binary Quantum Communication Based on Squeezed State

1.2.1 Dissipation Effect

The dissipation effects are studied for G=0.8, 0.5, 0.2, and 0 with $\alpha^2 = 3$ and N_{th}=2. Three results are represented: phase-space diagram, amplitude scan, and histogram for marginal probability distribution of the amplitude as shown in Figures 2-4, respectively.

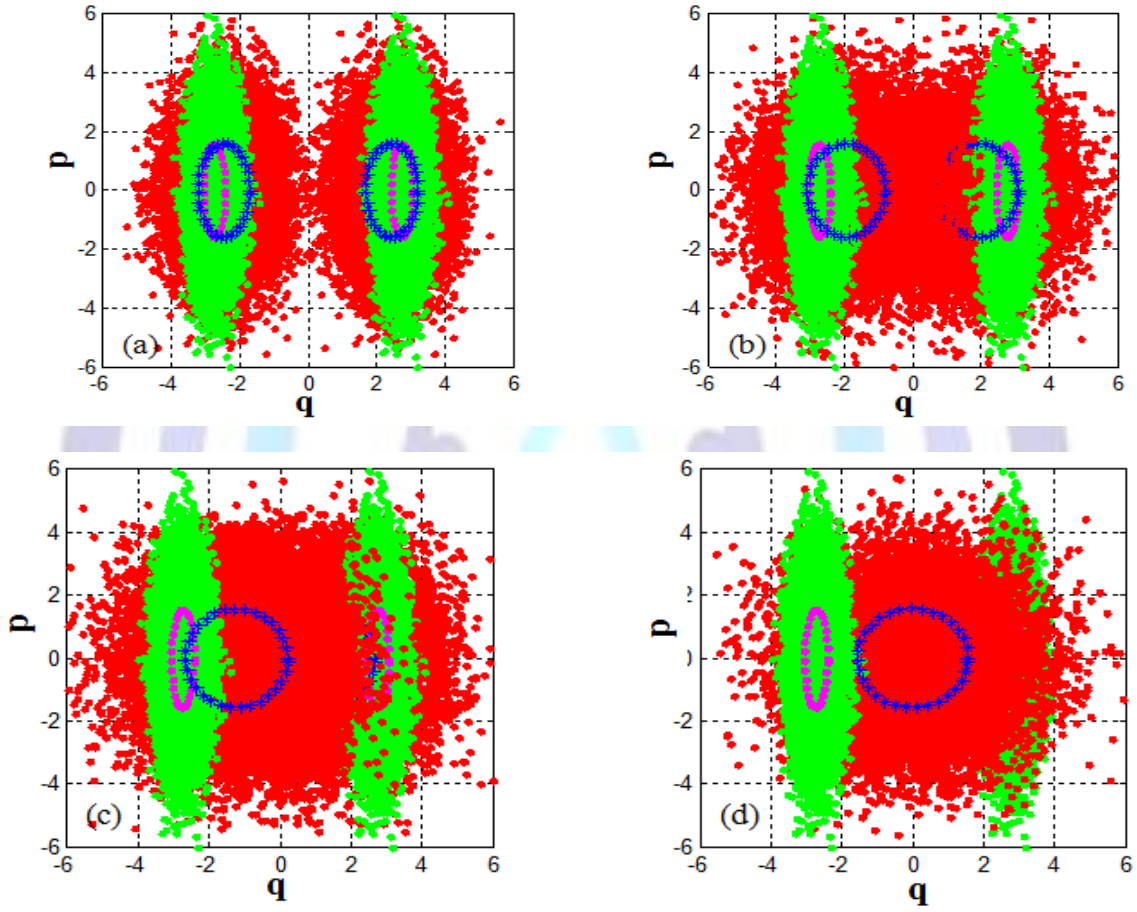

Figure 2: Phase-space simulation results for $\alpha^2 = 3$, N_{th}=2 and (a) G=0.8. (b) G=0.5. (c) G=0.2. (d) G=0.

Figure 2 represents the evolution of the state during transmission when G evolves from 0.8 to 0. There is a strong overlap occurring in the cases of G=0.5 and 0.2 and the state is entirely disappeared when G=0 where a new thermal state is obtained.

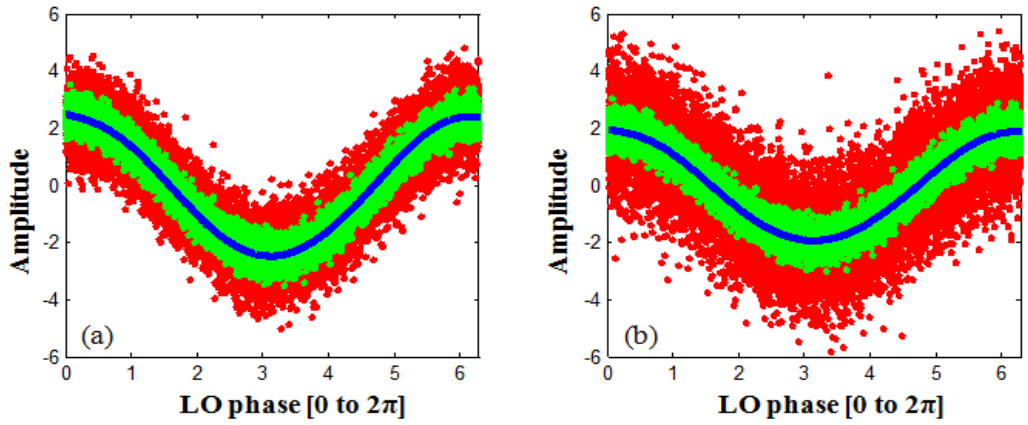

ISSN 2277-3061

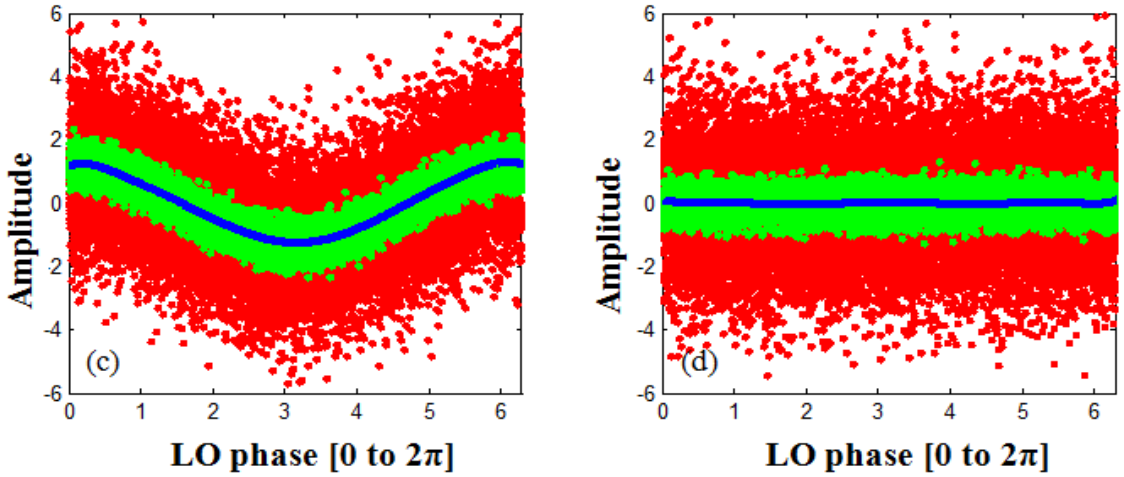

Figure 3: Amplitude scan simulation results for $\alpha^2 = 3$, N_{th}=2 and (a) G=0.8. (b) G=0.5. (c) G=0.2. (d) G=0.

The homodyne traces of Figure 3 shows the destruction of the squeezed coherent state due the dissipation effect. Moreover, the fixed number of the thermal noise plays a sophisticated role when the two states interfere thus the amplitude of the sine wave fitted curve decays more and more when G increases and becomes a line when G=0.

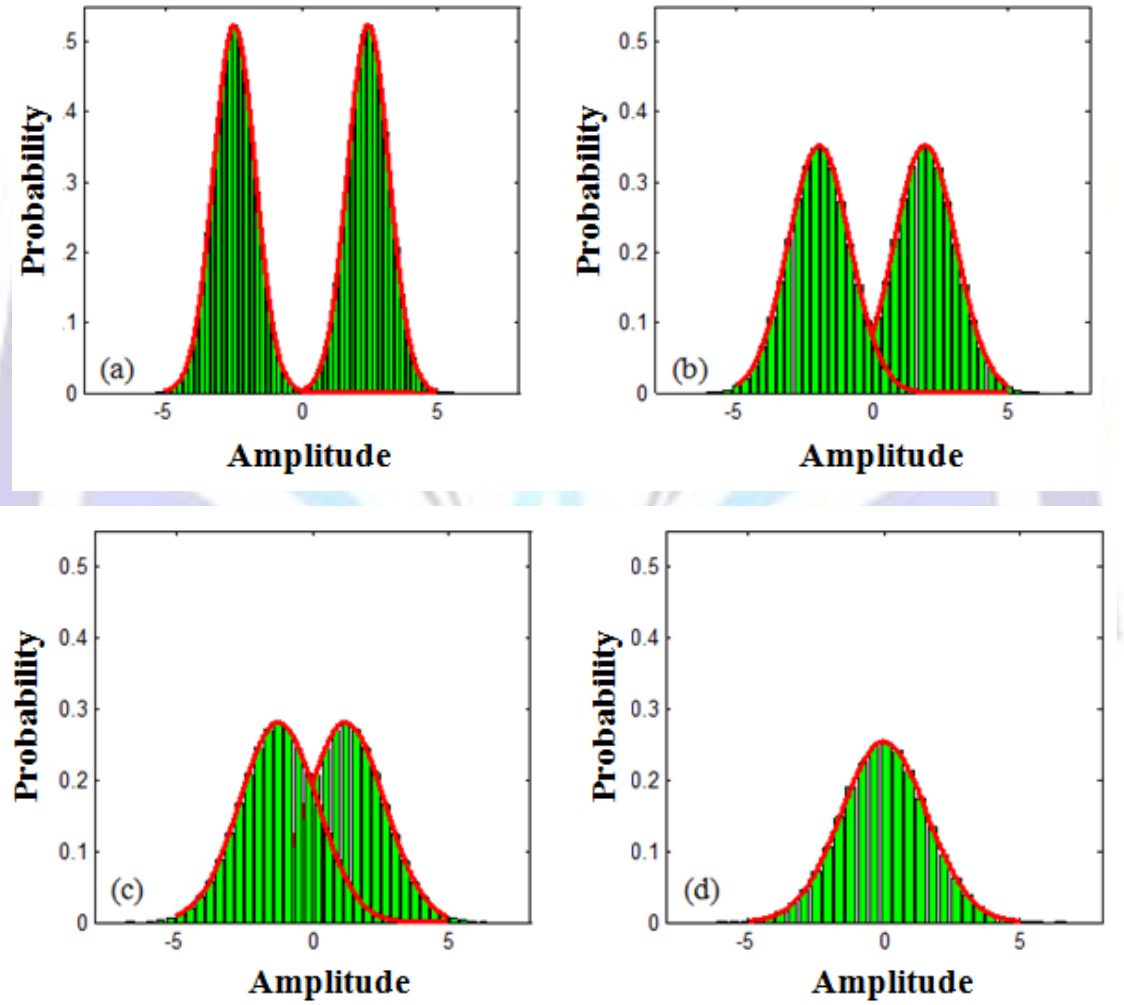

Figure 4: Probability simulation results for $\alpha^2 = 3$, N_{th}=2 and (a) G=0.8. (b) G=0.5. (c) G=0.2. (d) G=0.

The marginal probability distributions of the amplitude indicate that as the dissipation increases the amplitude of the state decreases as shown in Figure 4. They have Gaussian shapes with means 2.46, 1.94, 123 and 0 and standard deviations of 0.76, 1.14, 1.42, and 1.58, respectively.

1.2.2 Thermal Noise Effect

In this simulation, the parameters $\alpha^2 = 3$ and G = 0.5 are used while N_{th} is taken as independent parameter, N_{th} = 3, 4, 5 and 6. The effects are shown in Figures 5-7 representing the phase-space diagram, amplitude scan, and the probability of the amplitude, respectively.

The phase-space quadrature in Figure 5 explains that the increase of the thermal noise with constant G degrades the performance of the system and the receiver will be unable to discriminate the states. Increasing the thermal noise will increase the variance of the state as shown in Figure 5 by the blue ellipse that enlarges as N_{th} increases.

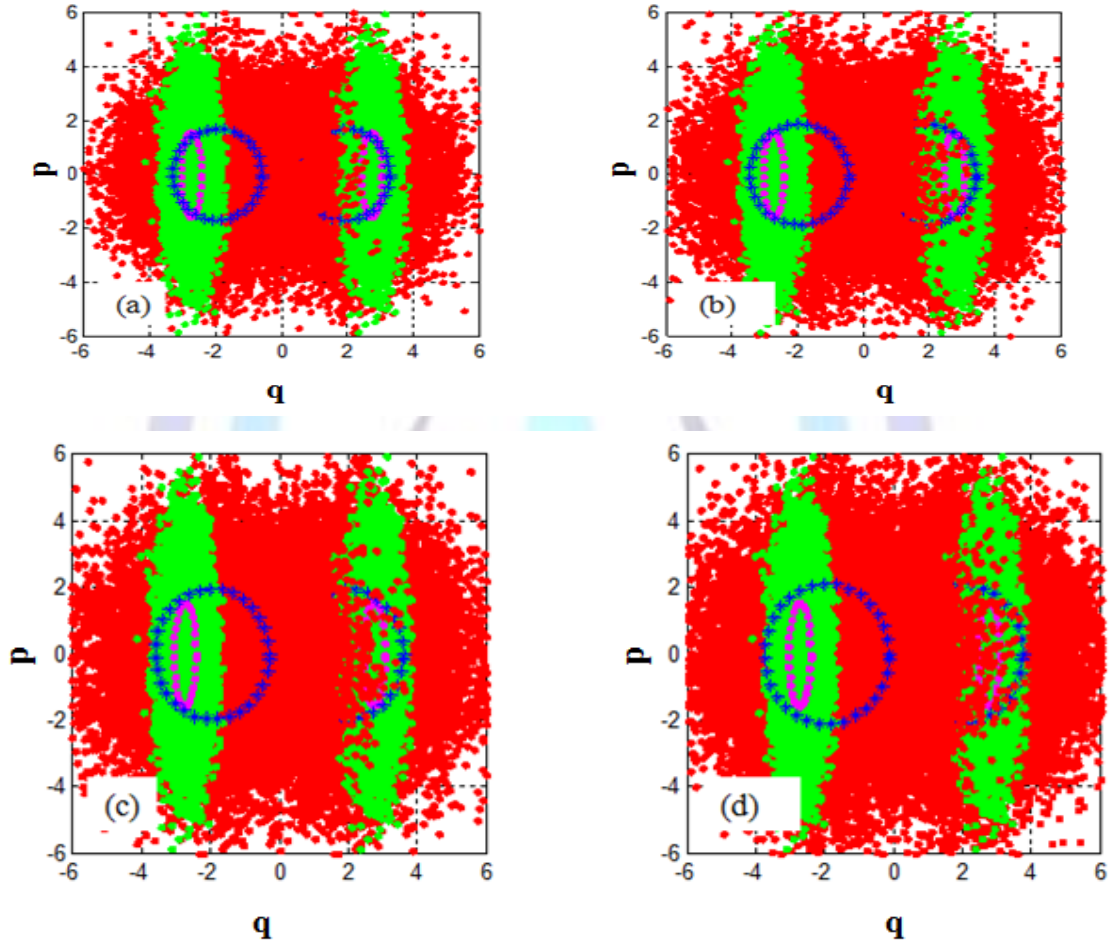

Figure 5: Phase-space simulation results for $\alpha^2 = 3$, G = 0.5 and (a) N_{th}=3. (b) N_{th}=4. (c) N_{th}=5. (d) N_{th}=6.

The blue line in Figure 6 is still unchanged as N_{th} increases due to the fact that the expectation of the state is constant for all cases. This is due to the fact that the evolved amplitude is independent on N_{th} and only depends on G. On the other hand, the fluctuations due to thermal noise increases by increasing N_{th} and the new state is a mixed state from the squeezed coherent state and the thermal state. The mixed state is a Gaussian state completely defined by its mean and variance.

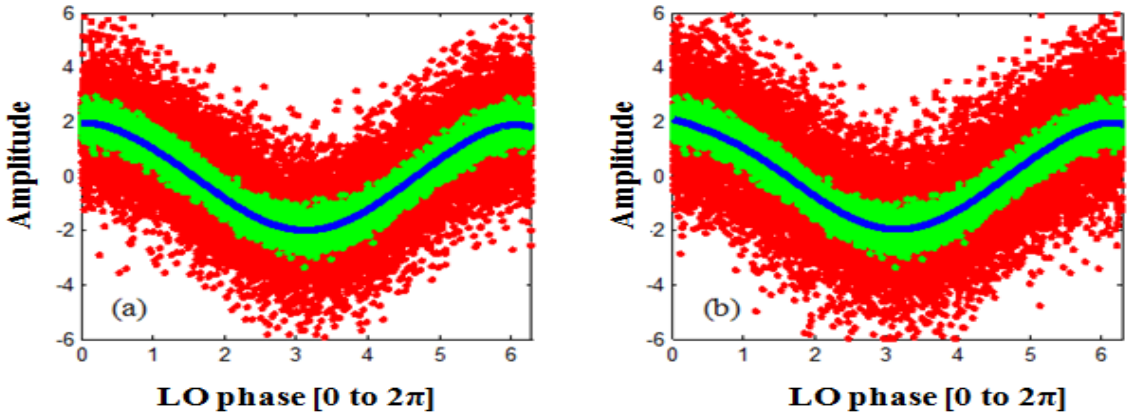

ISSN 2277-3061

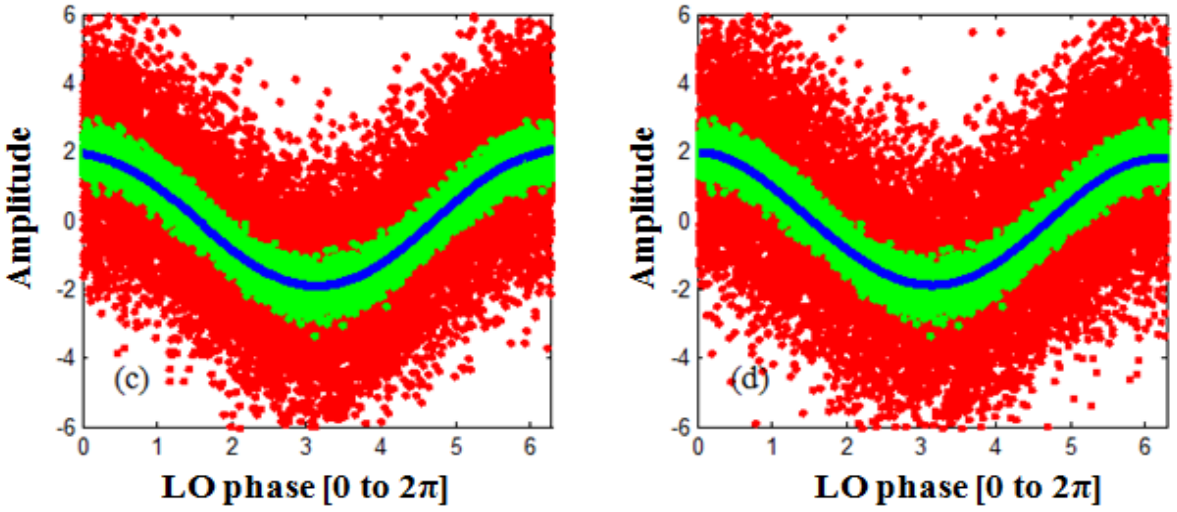

Figure 6: Amplitude scan simulation results for $\alpha^2 = 3$, G = 0.5 and (a) N_{th}=3. (b) N_{th}=4. (c) N_{th}=5. (d) N_{th}=6.

The marginal probability of the squeezed amplitude decreases by increasing N_{th} and the shape of the Gaussian profile becomes more and more stretch due the increase in the standard deviation of the state as N_{th} increases as shown in Figure 7. On the other hand, the mean remains constant for all the cases at 1.38 while the standard deviation has the values 1.34, 1.52, 1.67, and 1.82 for N_{th} = 3, 4, 5, and 6, respectively.

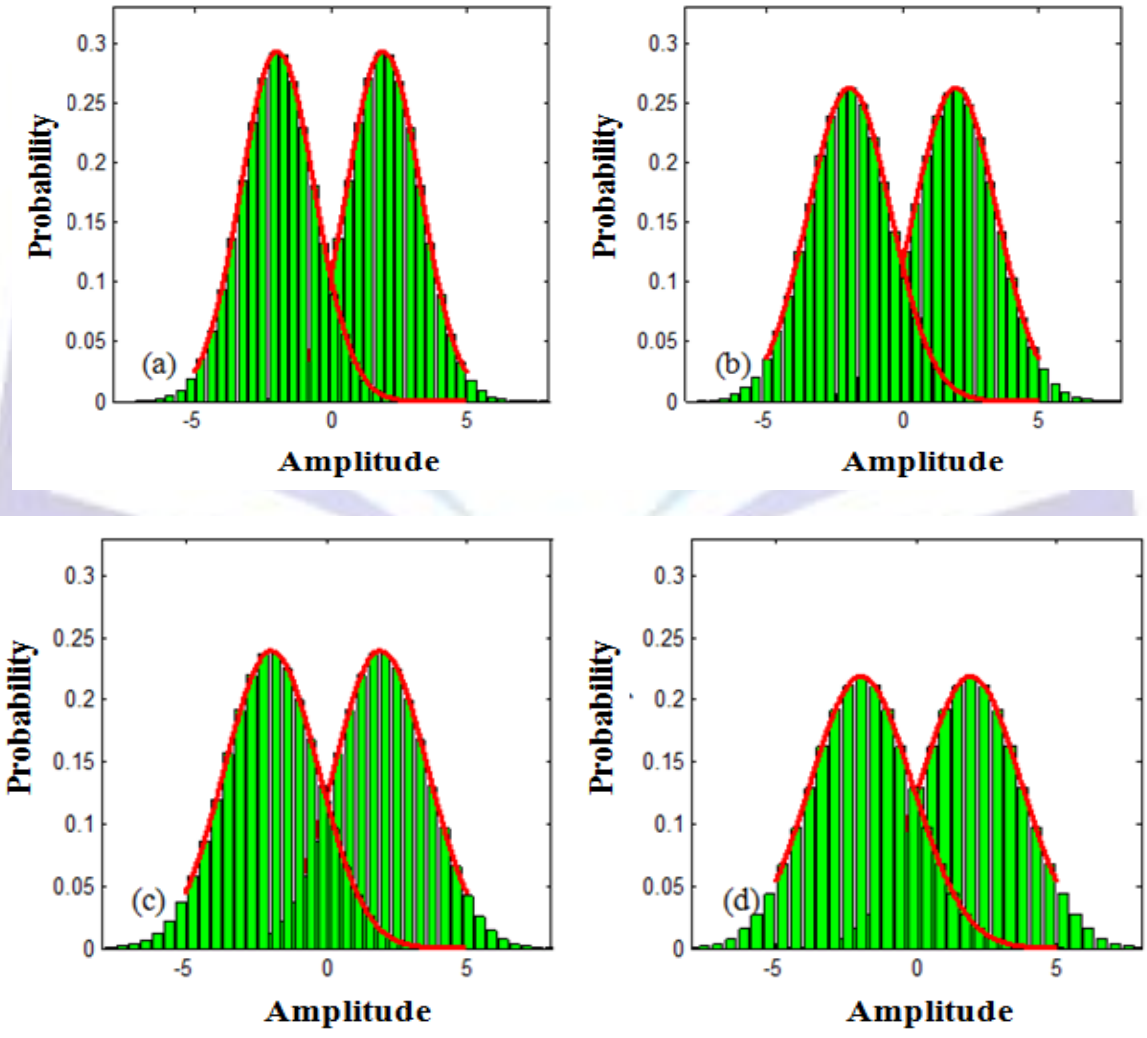

Figure 7: Probability simulation results for $\alpha^2 = 3$, G = 0.5 and (a) N_{th}=3. (b) N_{th}=4. (c) N_{th}=5. (d) N_{th}=6.

1.3 Error Probability

The performance of the system can be evaluated by computing the error probability of the transmitted state in the presence of dissipation and thermal noise. The error probability to discriminate between the two states at the receiver for N_{th} =0, 1, 2, 3, and 4 with varying G is shown in Figure 8.

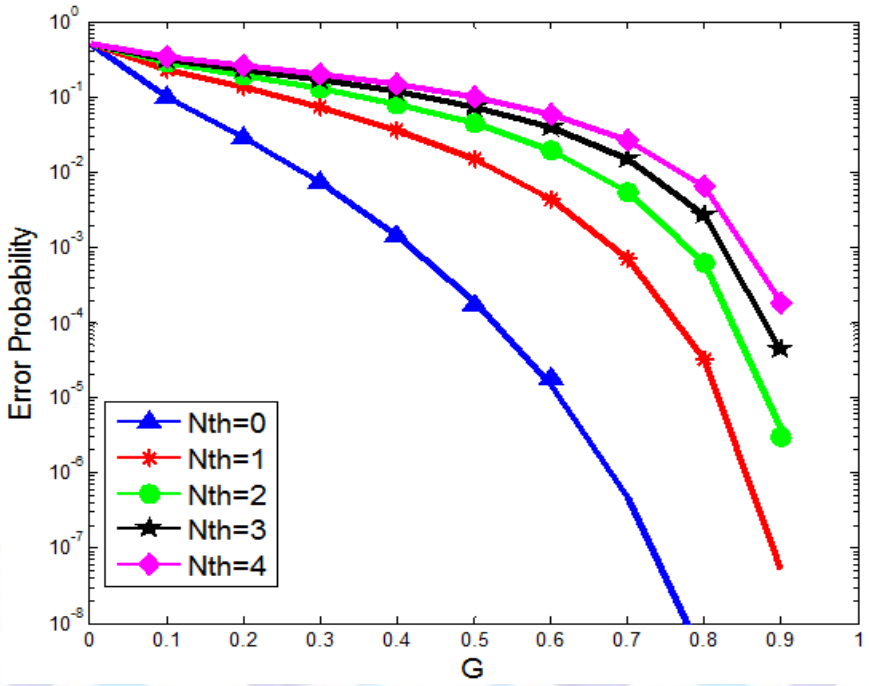

Figure 8: Error probability versus dissipation for $\alpha^2 = 3$ and different values of N_{th}. The circles are the simulation results and the solid lines represent the theoretical results.

The error probability increases as the dissipation increases as displayed in Figure 8. At N_{th}=0, the error probability is 6×10^{-7} for G=0.7 while for G=0.5, $P_e = 1.867 \times 10^{-4}$ as represented by the red curve. The error increases with increasing the dissipation until G=0 where the error becomes maximum and the state is evolved to the thermal state.

Figure 9 explains the effects of increasing the number of photons α^2 at N_{th} =2, when G varies from 0 to 1. α^2 has a crucial impact on the channel transmission. For $\alpha^2 = 7$ photons, the error probability is remarkable $P_e = 3.05 \times 10^{-10}$ for a dissipation of 50%. Moreover, P_e slightly decreases at G increases. For example, when G=0.3, $P_e = 2.067 \times 10^{-5}$ while for a small average number of photons, P_e saturates after certain value of G.

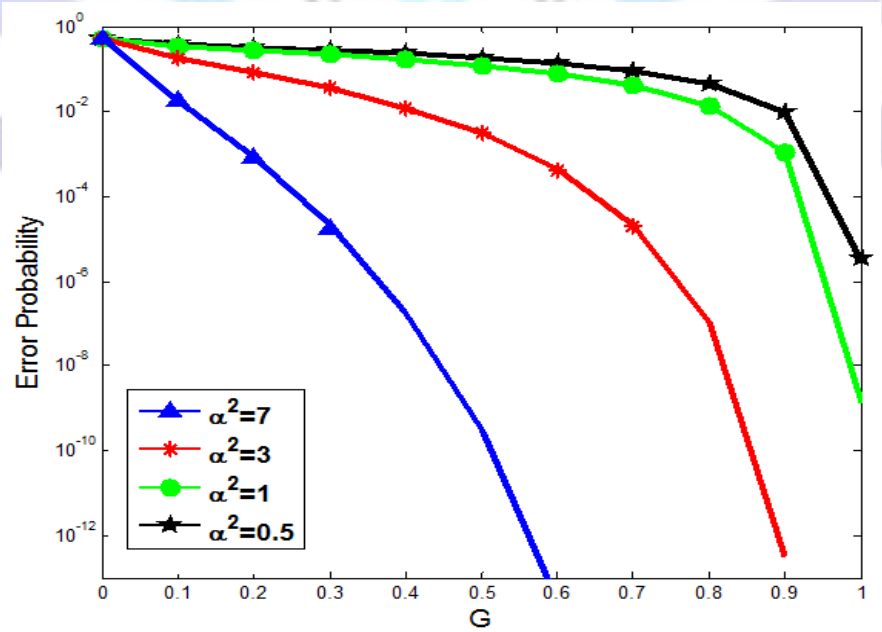

Figure 9: Error probability versus dissipation for $N_{th} = 2$ and different values of α^2. The circles are the simulation results and the solid lines represent the theoretical results.

Finally, Figure 10 illustrates the error probability to receive 0 while sending 1 in a binary quantum communication channel. In this figure at $\alpha^2 = 3$ and N_{th} is varied, four curves are given representing the error probability for G=0.8, 0.5, 0.2 and 0. If the channel is considered with little dissipation as for G=0.8, then the error probability for the squeezed state is remarkable and equals to 3.5×10^{-9}, 3.3×10^{-5} and 4×10^{-4} for N_{th}=0, 1 and 2, respectively. For G=0.5 and 0.2, the error probabilities are 1.94×10^{-4} and 2.8×10^{-2} when N_{th}=0, 1.4×10^{-2}, and 0.13 when N_{th}=1, and 4.3×10^{-2} and 0.19 when N_{th}=2. Moreover, the error probability is 0.5 for all N_{th} when G=0.

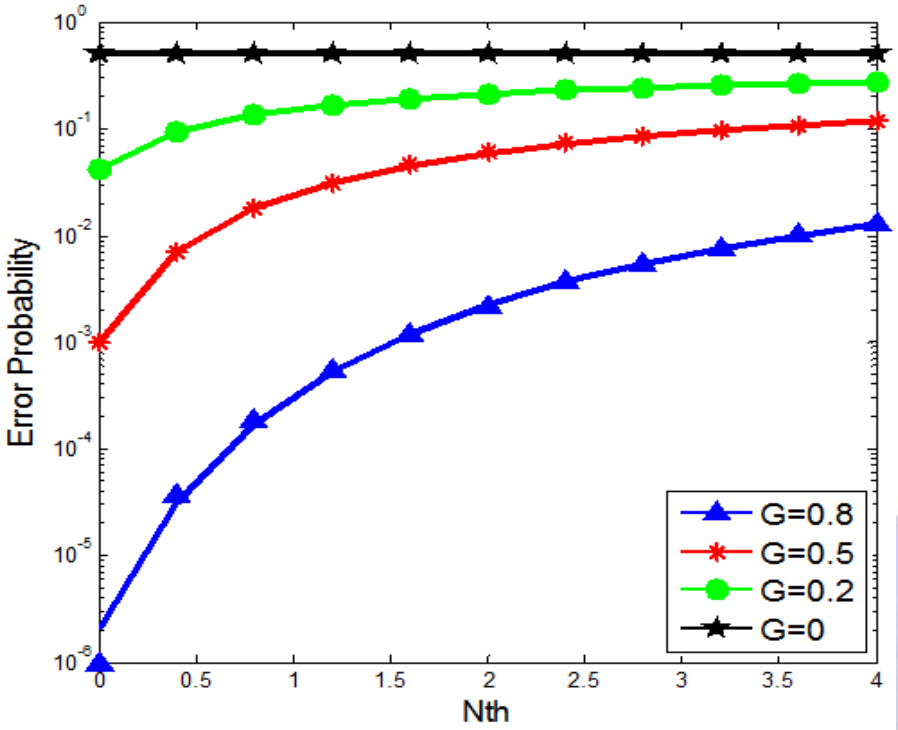

Figure 10: Error probability versus thermal noise for $\alpha^2 = 3$ and different values of G. The circles are the simulation results; the solid lines represent the theoretical results.

2 NUMERICAL and EXPERIMENTAL RESULTS

1.1 Numerical Results

The stability of the ring resonator m is not constant. It changes according to the focal length of the thermal lens f_{th} that varies with the pump current as shown in Figure 11a. In fact, all the characteristics of the resonator change with f_{th} involving the waist inside the active medium as illustrated in Figure 11b.

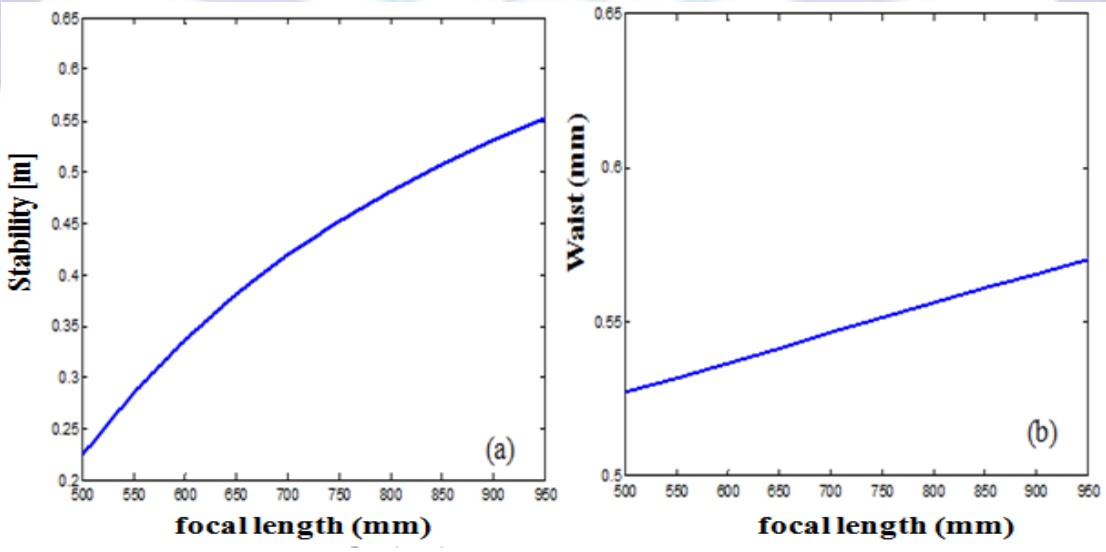

Figure 11: Ring resonator characteristics. (a) Stability as a function of the thermal lens. (b) Waist inside the active medium.

As shown in Figure 11a, the resonator is considered very stable because $m < 1$. For the thermal focal length range between 500 and 950 mm, m is between 0.224 and 0.551. Moreover, the waist varies from $527\ \mu m$ to $570\ \mu m$ as f_{th} varies from 500 to 950 mm, respectively.

Next, the PPLN crystal needs to be placed at the focusing place where the waist is minimum as shown in Figure 12.

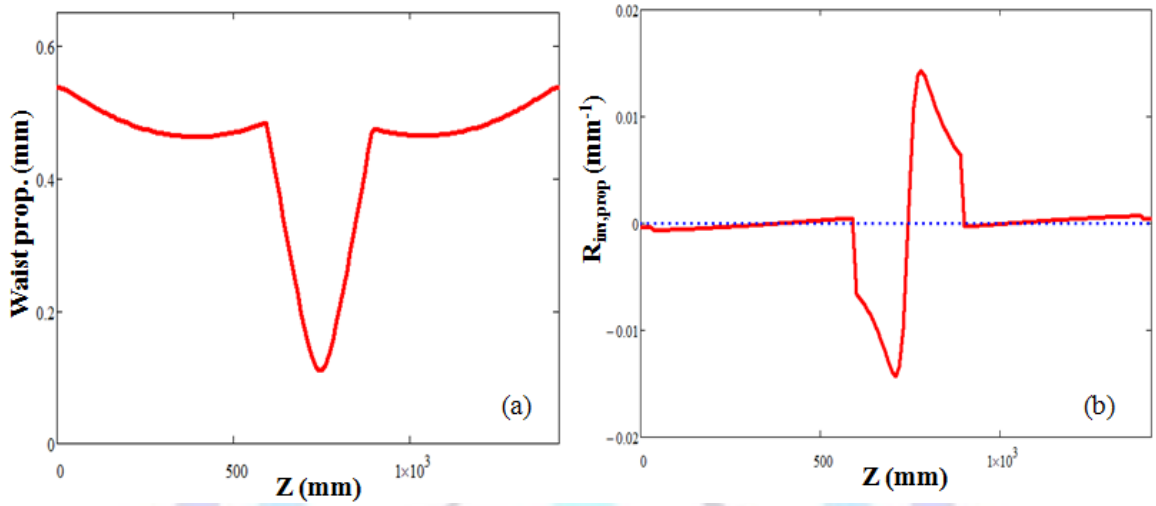

Figure 12: Propagation of the beam through the cavity. (a) Waist of the beam. (b) Inverse radius of curvature of the beam.

The maximum focusing is obtained at $z = 742\ mm$ where the spot size $101\ \mu m$ as shown in Figure 12a. This position corresponds to the middle distance between mirrors M_3 and M_4. The wave travelling between M_3 and M_4 is a plane wave. The inverse radius of curvature is in the range of $4.5 \times 10^{-4}\ mm^{-1}$ and $3.2 \times 10^{-4}\ mm^{-1}$ for $z = 590\ mm$, and $900\ mm$, respectively, as indicated in Figure 12b.

1.2 Experimental Results

2.2.1 Determination of the Quasi-Phase Matching Temperature

First, the temperature at which the QPM is achieved through the PPLN crystal is determined in order to obtain the maximum optical power for generating the second harmonic (532 nm). Table 1 shows the measured voltages and powers of the second-harmonic wave at different temperature and fixed-pump current of 19A.

Table 1: Second harmonic output power at different temperature.

Temperature (^oC)	V_{out} (mV)	P_{out} (mW)
68.250	125.00	7.8125
68.500	140.00	8.7500
68.750	140.00	8.7500
69.000	160.00	10.000
69.250	160.00	10.000
69.500	150.00	9.3750
69.750	150.00	9.3750
70.000	150.00	9.3750
70.250	150.00	9.3750
70.500	125.00	7.8125
70.750	120.00	7.5000

71.000	120.00	7.5000

Second, a graph representation of these results is shown in Figure 13. Using KaleidaGraph program to plot the characteristics of the output power of the second harmonic versus the temperature using the measurement data given in Table 1.
The curve shown in Figure 13 is approximately a quadrature one with a maximum temperature of 69.5 ℃ achieving at the center of the curve. Thus, QPM is achieved at 69.5 ℃ for a pump current of 19A. The maximum second-harmonic power is obtained at this temperature. From now, the temperature of the PPLN will be fixed at 69.5 ℃.

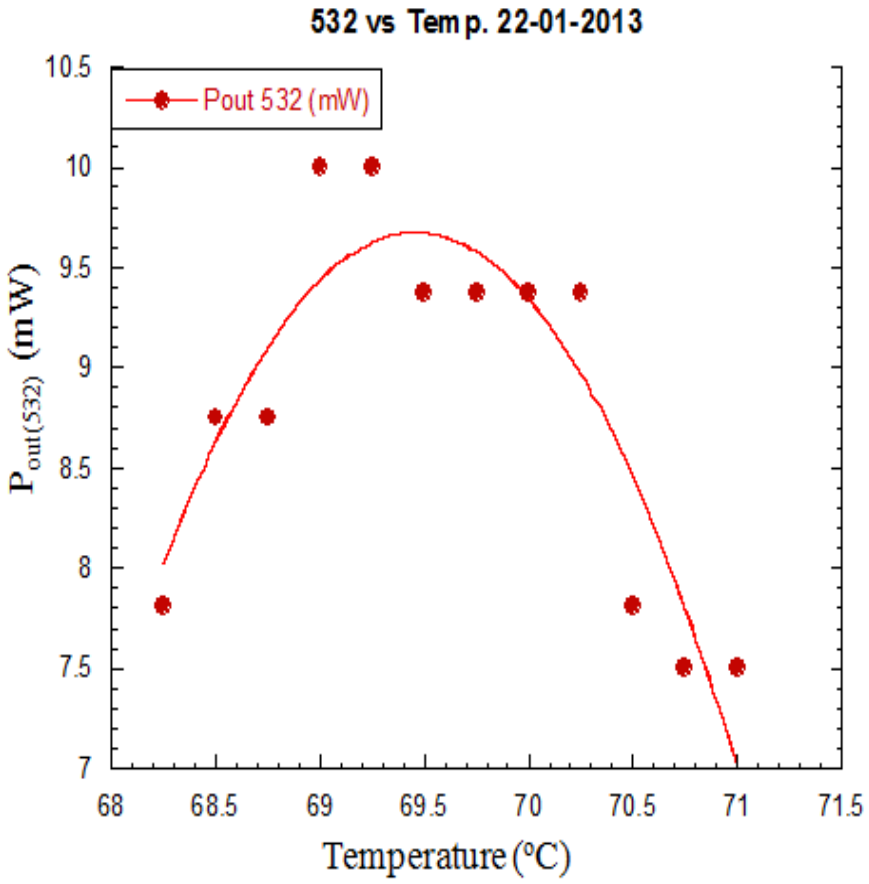

Figure 13: Second-harmonic optical power versus temperature at a pump current of 19A.

2.2.2 First and Second Harmonic Output Powers

The pump current is varied from the threshold level 16.3A (when the lasing is initiated) to 22A. At each pumping current, the output powers of the first and second harmonic wavelengths (P_{out} (1ω) and P_{out} (2ω)) are measured via PD_1 and PD_2, respectively. Additionally, the power inside the resonator is also measured. Table 2 contains the output voltages that measured by PD_1 and PD_2 and their corresponding incident optical powers P_{in}. The graphical representation is shown in Figure 14 with the two vertical axes representing the powers of the second-harmonic and the power inside the resonator.

Table 2: Voltages and Powers of 1ω and 2ω.

Pump (A)	V_{out} (1ω) (V)	V_{out} (2ω) (V)	P_{out} (1ω) (mW)	P_{out} (2ω) (mW)	P_{in} (W)
16.30	0.00	0.00	0.00	0.00	0.00
16.50	0.10	0.01	27.03	0.63	1.00
17.00	0.25	0.15	67.57	9.38	2.50

18.00	0.63	0.73	170.27	45.63	6.31
19.00	0.90	1.40	243.24	87.50	9.01
20.00	1.16	2.25	313.51	140.63	11.61
20.50	1.30	2.90	351.35	181.25	13.01
21.00	1.45	3.70	391.89	231.25	14.52
21.50	1.60	4.50	432.43	281.25	16.02
22.00	1.70	5.20	459.46	325.00	17.02

Figure 14 illustrates how the first and second harmonic powers increase as increasing the pump current. From this graph, one can see that the optical power of the first harmonic varies approximately linearly with the pumping current as well as the power inside the cavity, which is normally a consequence of the characteristics of the laser operating above threshold. However, this is not the case for the second harmonic where the power changes approximately in a quadratic manner against pumping current. In addition, the curve in Figure 14 gives a wide reliability to choose the suitable power required to generate the squeezed light. One can observe that when the current increases from 16 to 22A, the second harmonic power increases from 0 to 325 mW.

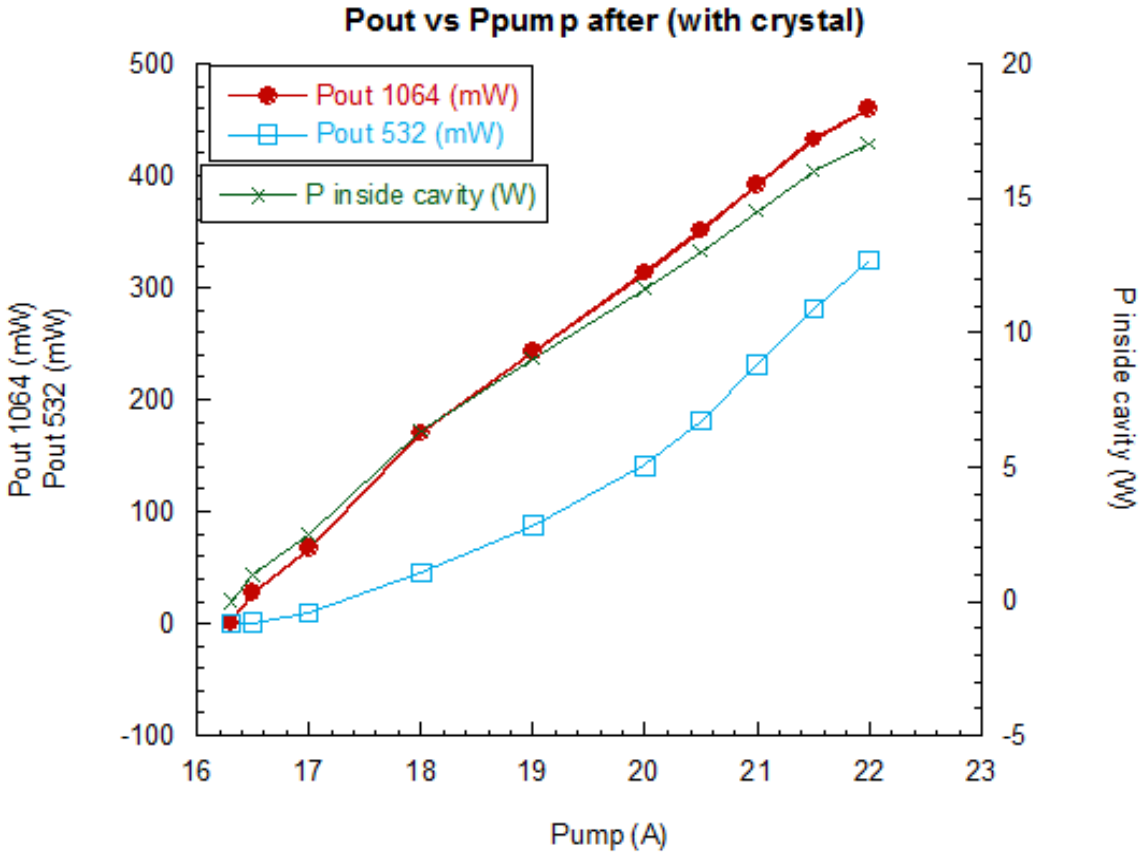

Figure 14: First harmonic, second harmonic, and cavity powers versus pumping current.

2.3 Squeezed Cavity: Numerical Results

2.3.1 Refractive Indices Representation

To achieve NCPM in the LNB crystal, one has to determine the temperature at which the extraordinary and the ordinary refractive indices are matching. The refractive indices as a function of the temperature and the wavelength are represented in Figures 15a and 15b.

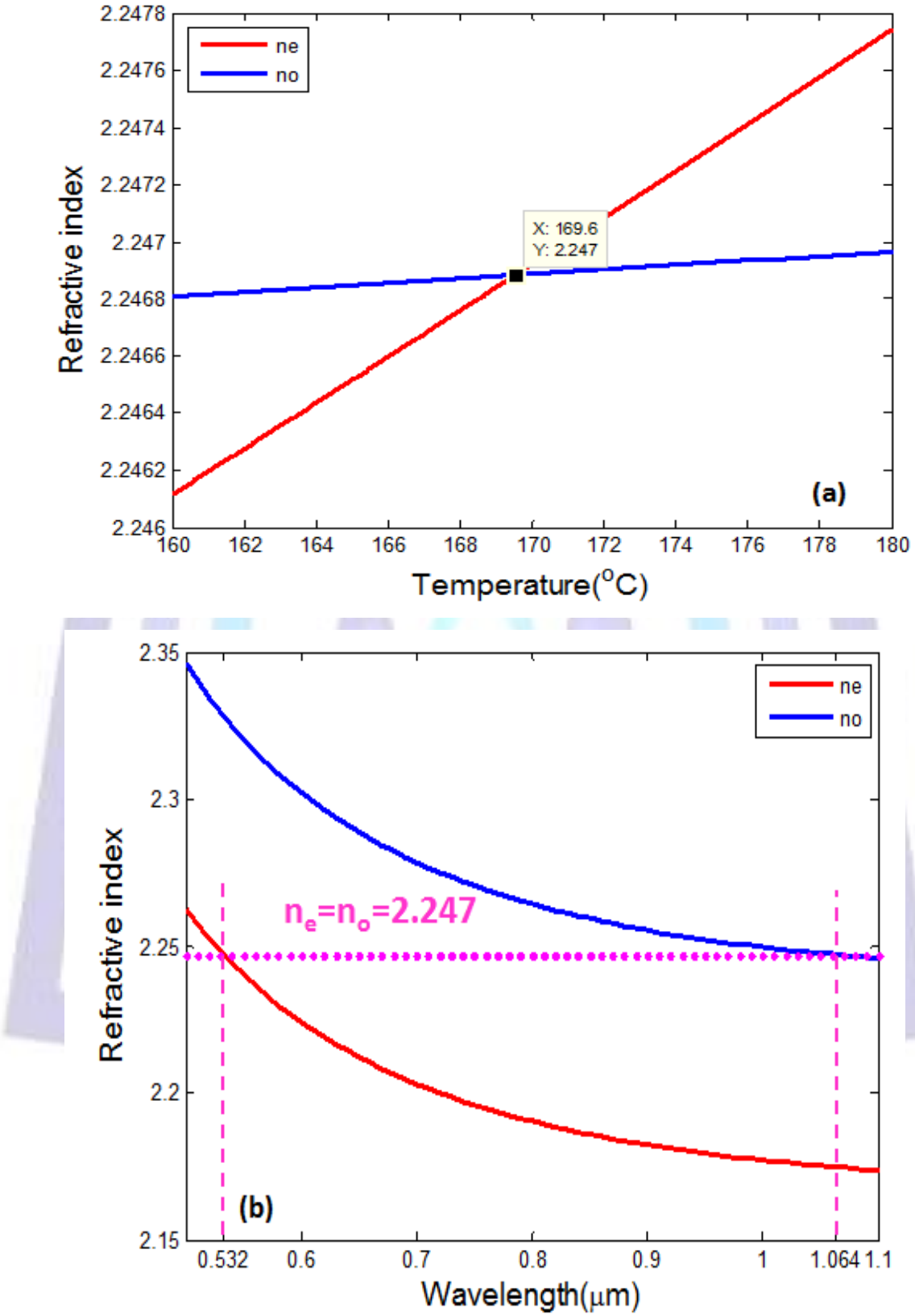

Figure 15: Refractive indices representations. (a) As a function of the temperature. (b) As a function of the wavelength.

The extraordinary and the ordinary refractive indices curves are intersected at 169.6℃ for $n_e(2\omega) = n_o(\omega) = 2.247$ as shown in Figure 15a. At 170℃, the NCPM is investigated and Figure 15b confirms this results (i.e., $n_e = n_o = 2.247$ for the wavelengths 532 nm and 1064 nm, respectively).

2.3.2 FSR and Stability Results

The effective length of the squeezed resonator $L_{eff} = 45.47\ mm$ and the free spectral range $FSR_{sq} = 3.3\ GHz$. The stability of the resonator $m_{sq} = 0.658$ which indicates that the resonator is stable.

2.3.3 First Harmonic Propagation Results

Figure 16 shows the propagation of the beam waist along the cavity length. It is found that the waist of the first harmonic varies from $207.6\ \mu m$ at M_{S1} to $49.2\ \mu m$ at M_{S2}. The region with the more interest is between 20 and 30 mm where the crystal is located. The waist in this region of length L_S varies from $52.8\ \mu m$ to $40.2\ \mu m$ with a value of $42.96\ \mu m$ at the center of the crystal. Thus, the beam exhibits fluctuation through propagation inside the crystal.

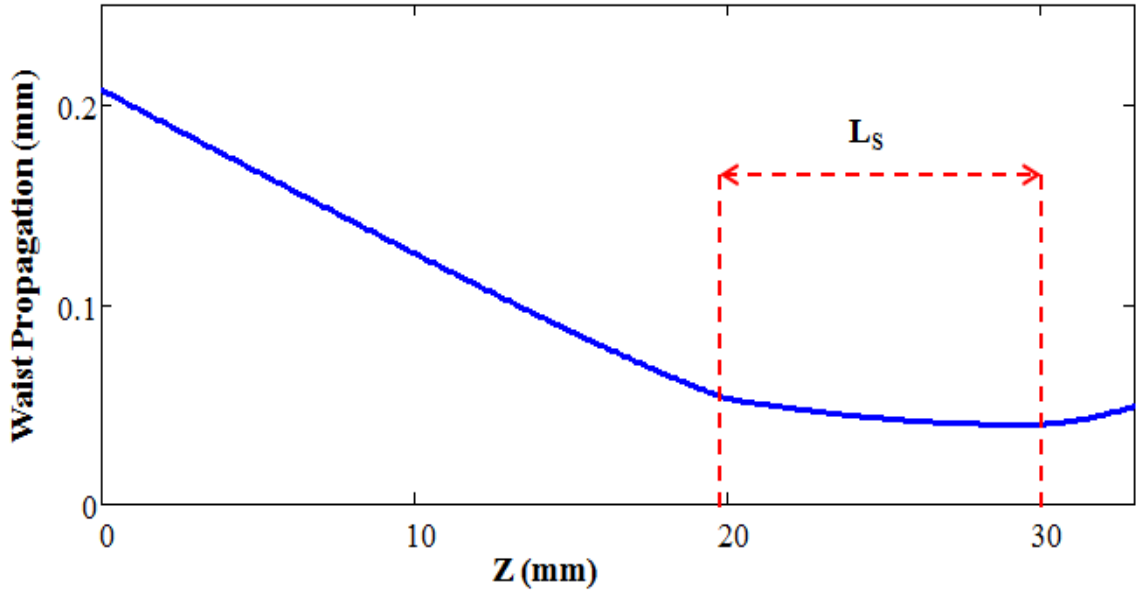

Figure 16: Propagation of the beam along the axis z.

The inverse radius of curvature is represented in Figure 17. Note that the radius of curvature varies between the -25 mm and 10 mm that correspond to the radii of curvature of M_{S1} and M_{S2}, respectively. Inside the crystal, the wave is not plane and the radius of curvature fluctuates between -9.57 mm at z=20 mm to 133.8 mm at z=30 mm with minimum value 2.474×10^3 mm at z=29.1 mm.

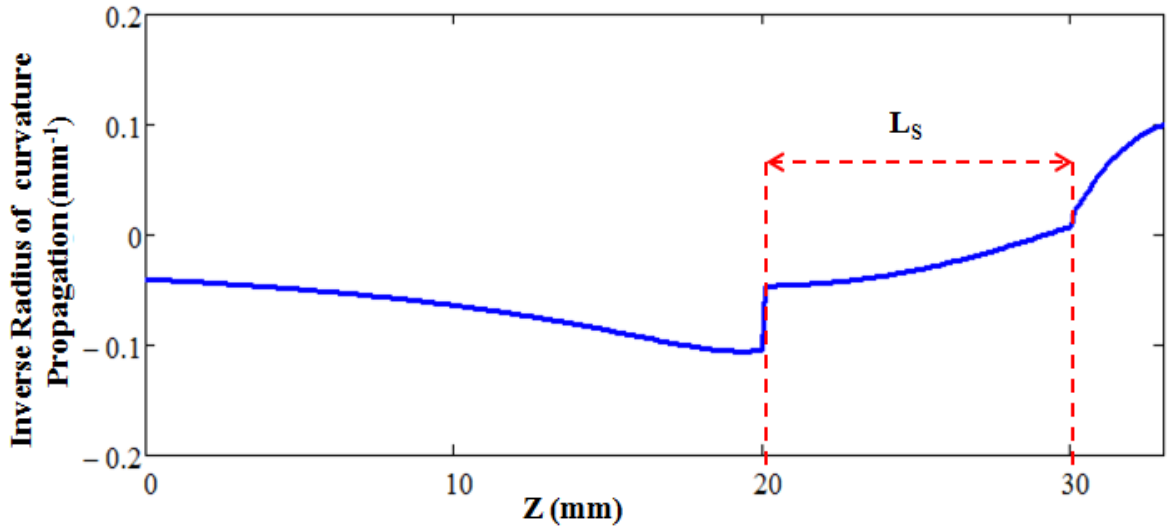

Figure 17: Inverse radius of curvature propagation through the cavity.

2.3.4 Second Harmonic Propagation Results

The second harmonic beam should be well inside the first harmonic beam in order to generate the squeezed light as shown in Figure 18.

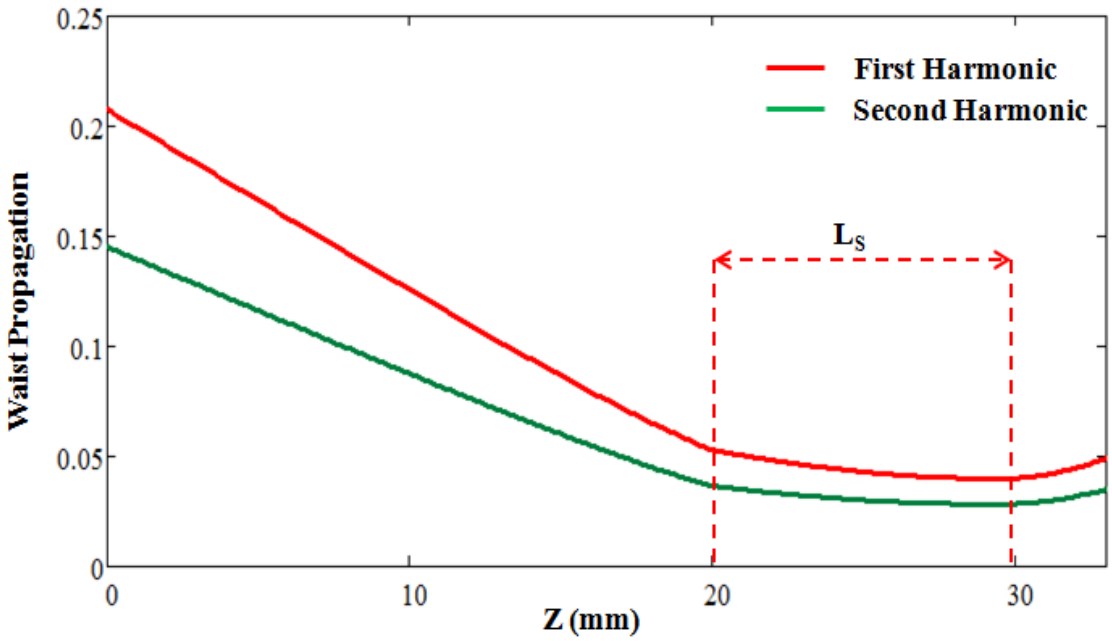

Figure 18: Waist propagation through the squeezed cavity.

The waist of the second harmonic varies from $145.27\ \mu m$ at the mirror M_{S1} to $35\ \mu m$ at the mirror M_{S2} with variation inside the crystal from $36.54\ \mu m$ at $z = 20\ mm$ to $28.48\ \mu m$ at $z = 30\ mm$. The fluctuation of the second harmonic inside the crystal is about $8\ \mu m$ which is not significant and this is so important in the generation of the squeezed light. The waist of the pump beam should have an optimum value of $31.82\ \mu m$ in order to be well inside the seeded beam. The threshold intensity of the pumping beam in the OPO is $9.883 \times 10^7\ photons/cm^2$. Thus, the minimum threshold power required is 157 mW.

2.3.5 Squeezed Light Generation Results

First, one has to determine the frequency Ω at which the variance of the squeezed state is optimum. The squeezed variance as a function of Ω is shown in Figure 19. The curve has a quadrature shape at which the optimum squeezing -10.016 dB is obtained for Ω=0.

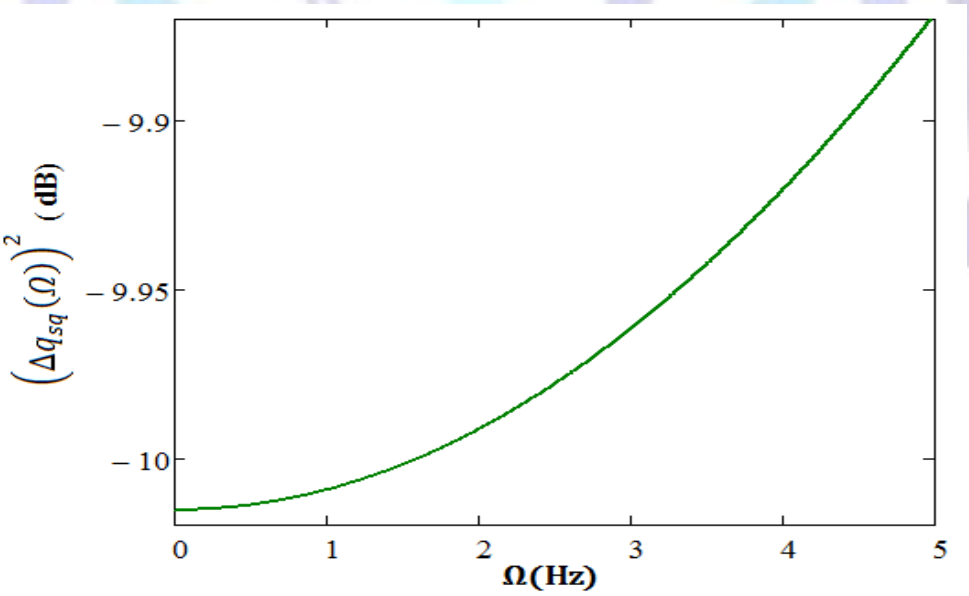

Figure 19: Squeezed variance as a function of the frequency.

Figure 20 illustrates the variation of the squeezed variance with the escape efficiency. The squeezing varies linearly with the variance. Therefore, it has a crucial effect on the generation of the squeezed state. For a zero frequency and a pump power of 0.5 W, the squeezed variance varies from $-3.0103\ dB$ at $\eta_{esc} = 0$ to $-17.084\ dB$ at $\eta_{esc} = 1$. Note that the quantum limit of the vacuum corresponds to a variance with zero escape efficiency.

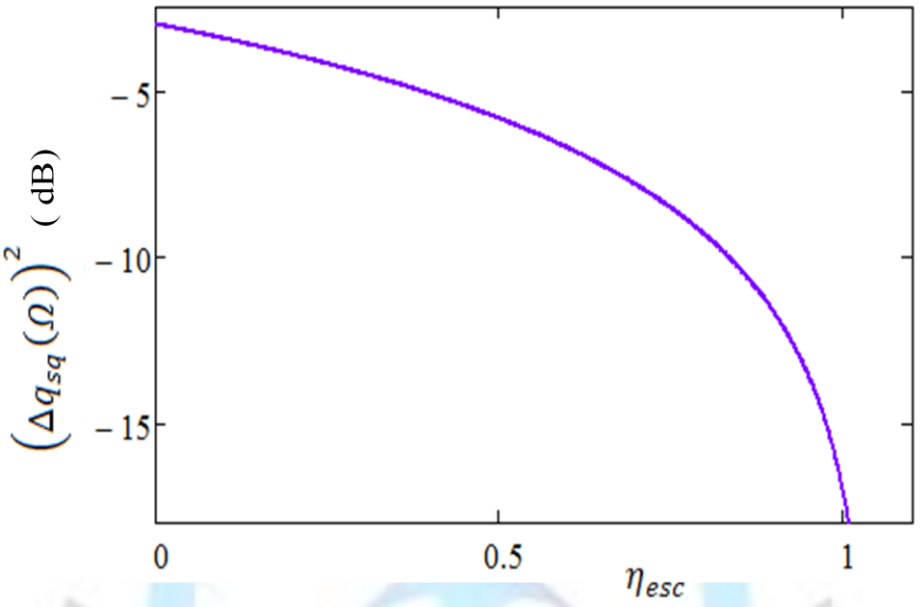

Figure 20: Squeezed variance as a function of the escape efficiency.

Finally, a representation of the squeezed and anti-squeezed variances as a function of the pump power is represented in Figure 21.

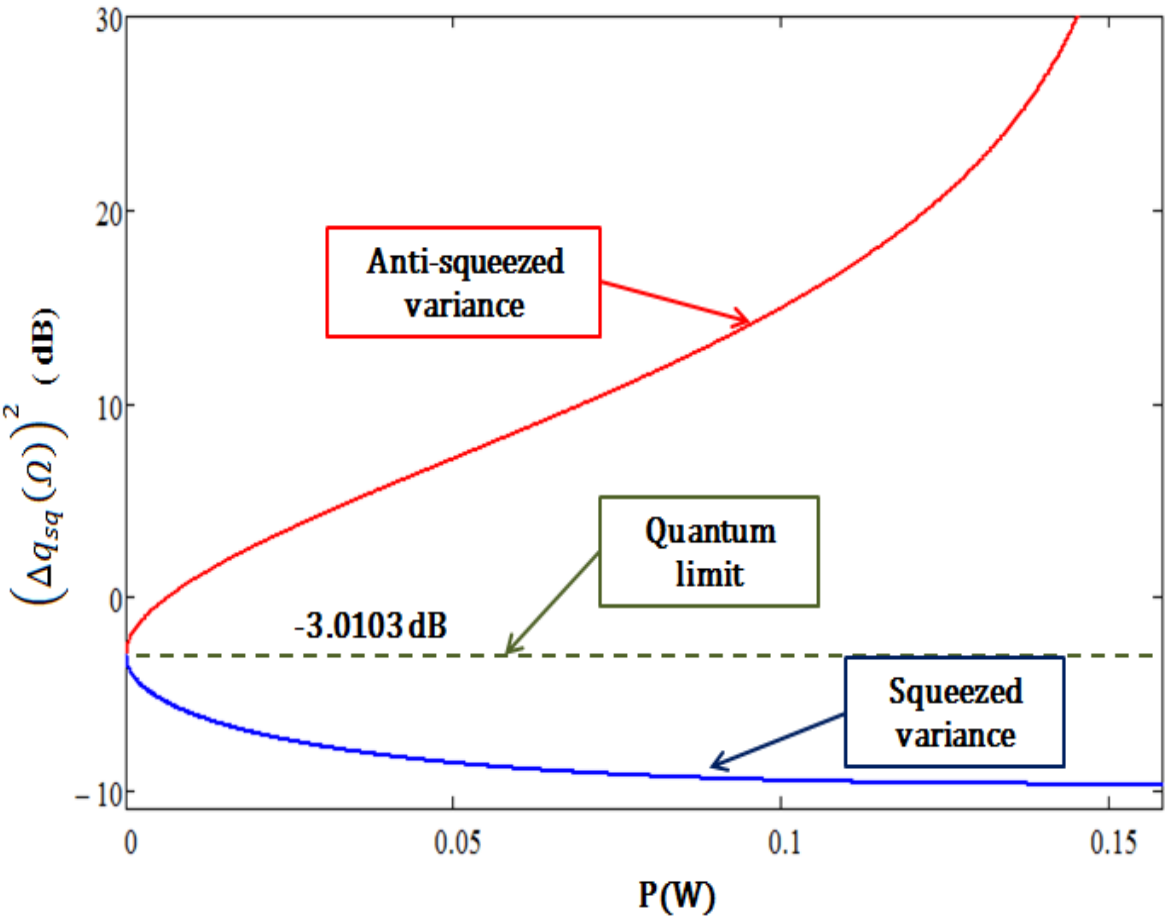

Figure 21: Squeezed and anti-squeezed quadrature versus pump power.

Figure 21 indicates that squeezing increases with increasing the power. Furthermore, the squeezed quadrature saturates below the threshold. Therefore, it is not necessary to increase the pump power up to the threshold. At an escape efficiency of 79.5%, the degree of squeezing for different values of the power is shown in Table 3.

Table 3: Squeezed and anti-squeezed quadrature versus pump power.

Pump power (mW)	Squeezed quadrature (dB)	Anti-squeezed quadrature (dB)
0	-3.01	-3.01
20	-4.10	5.71
40	-5.26	8.74
50	-5.63	10.15
60	-5.91	11.57
70	-6.13	13.02
80	-6.29	14.55
100	-6.53	17.97
120	-6.65	22.46

Table 3 indicates that the maximum squeezing below the quantum limit is obtained $(-6.29\ dB)$ at a pump power of 80 mW. The reduction of the squeezing for the pump power above 50 mW has a slowly variation due to the fact that the squeezed quadrature saturates below the threshold.

2.3.6 Pound-Drever-Haul Results

The error signal is fed to the piezoelectric in order to control the cavity length as shown in Figure 22 which displays two regions, one is above the resonance when the error is positive and the other is below the resonance when the error is negative. When the length of the resonator increases, the error increases hence more voltage is needed to be applied at the piezoelectric in order to return the cavity back to the resonance position and vice versa.

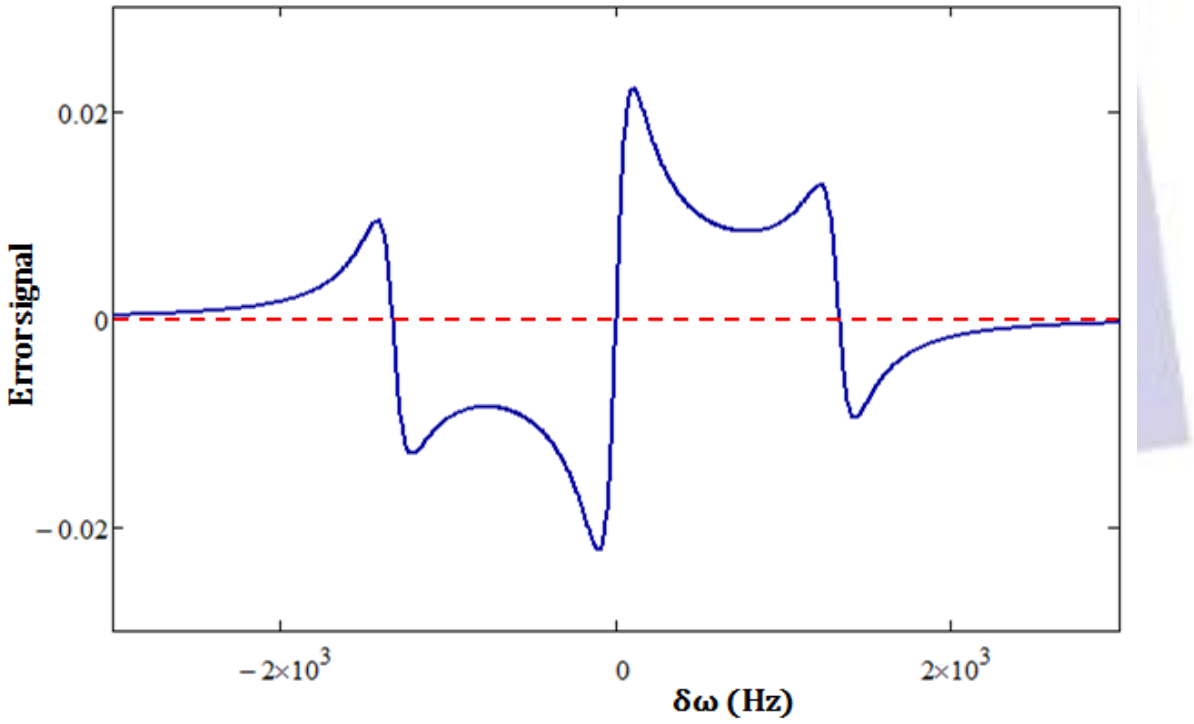

Figure 22: Pound Drever Haul Error signal.

2.3.7 Balance Homodyne Results

The homodyne trace represents the phase quadrature over the LO phase $\emptyset_\beta$ which varies from 0 to 2π as shown in Figure 23. At a pump power of 50 mW, the squeezed variance is -9.31 dB while the anti-squeezed is 11, 32 dB, which means that there is a noise reduction of -6.30 dB below the standard quantum limit versus a 14.54 dB above. This value is expected due the small value of the escape efficiency (79.5%) which depends on the apparatus involved in the setup such as the reflectivity of the output coupler and the internal losses.

ISSN 2277-3061

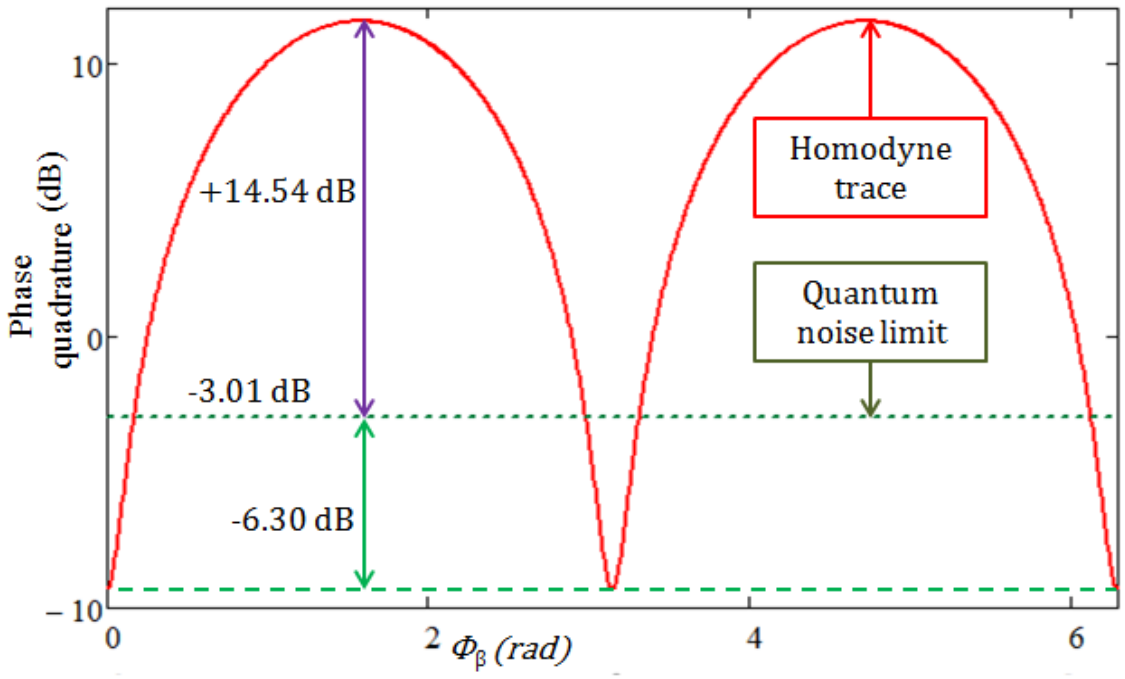

Figure 23: Homodyne trace for P=80 mW.

2 ERROR PROBABILITY COMPARISON

Here, a comparison is given from error probability point of view between the coherent and the squeezed states in the binary quantum communication system as shown in Figures 24-26.

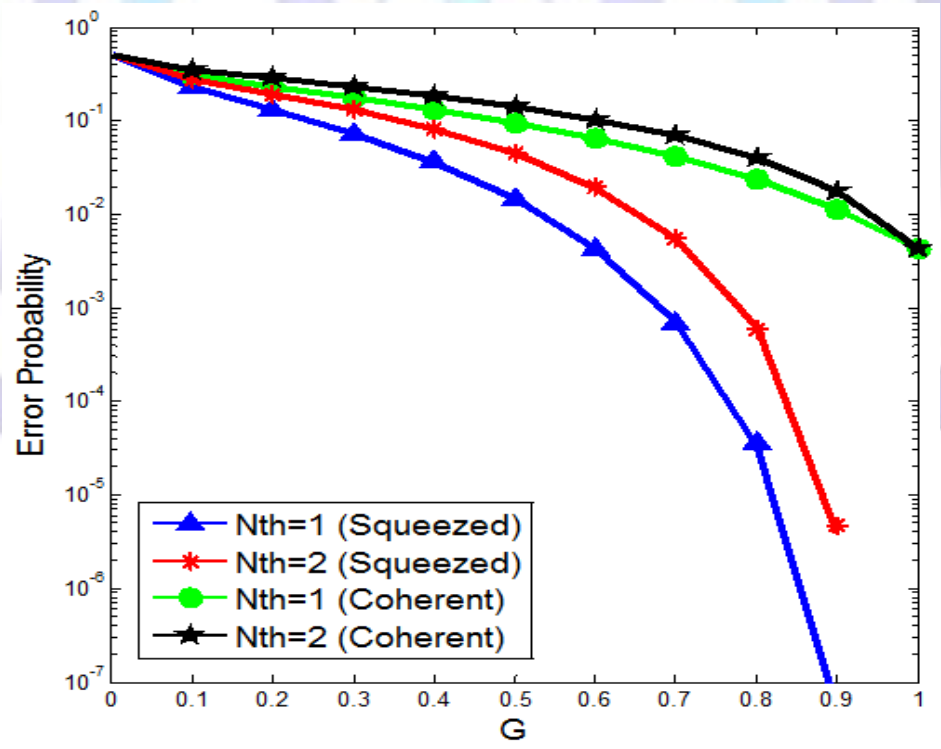

Figure 24: Simulation error probability comparison for $\alpha^2 = 3$ and N_{th}=1 and 2 with varying G. The circles are the simulation results; the solid lines represent the theoretical results.

Figure 24 shows a comparison between the squeezed and the coherent states for $\alpha^2 = 3$ and N_{th}=1 and 2 with varying G. Investigating this figure reveals that the error probability for both squeezed and coherent states has the same value $1/2$ when G=0. This is true because the two states will be evolved to the thermal state when t approaches infinity and hence the maximum error is obtained. For G=1 (i.e., without dissipation), the coherent state has an error probability of $4.26 \times$

10^{-3} for both N_{th}=1 and 2. The squeezed state has almost the same error, 4.34×10^{-3} for G=0.6, N_{th}=1 and 5.47×10^{-3} for G=0.7, N_{th}=2. Thus, the squeezed state overcomes the effect of dissipation imposed by the channel during transmission. Furthermore, the squeezed state with 3 photons and for a light dissipation may have an excellent error probability in the order of less than 10^{-7}.

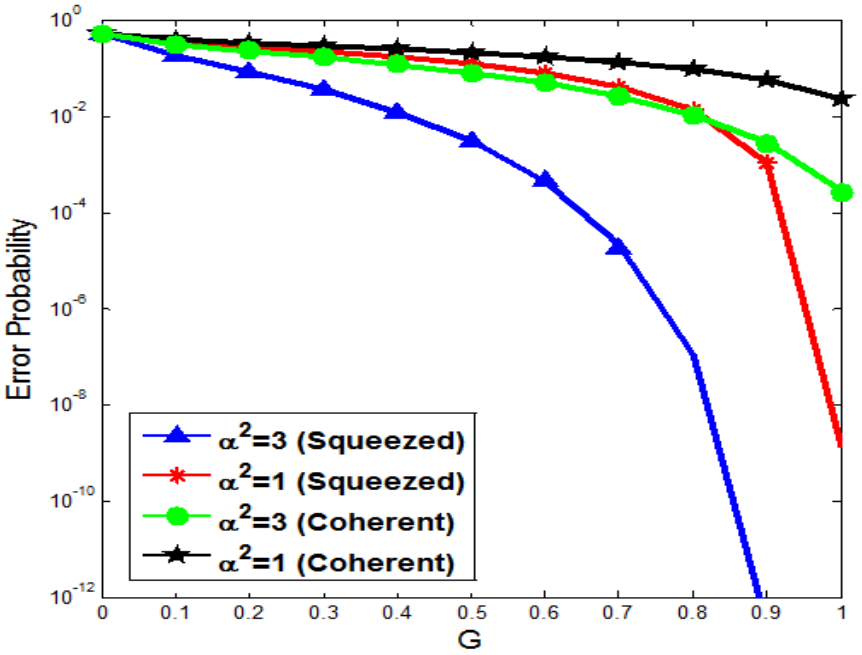

Figure 25: Simulation error probability comparison for $\alpha^2 = 1$, 3 and N_{th}=2 with varying G. The circles are the simulation results; the solid lines represent the theoretical results.

Figure 25 illustrates the error probability for two values of number of photons, $\alpha^2 = 1$ and 3. Here N_{th}=2 where G is varied between 0 and 1. For G=0.7, the error probabilities for the coherent state are 0.025 and 0.13 for $\alpha^2 = 3$ and 1, respectively. For the squeezed state, P_e is 2.4×10^{-5} and 0.04 for $\alpha^2 = 3$ and 1, respectively. Thus, the squeezed state enhances significantly the channel transmission performance and overcomes the environment effects and the dissipation.

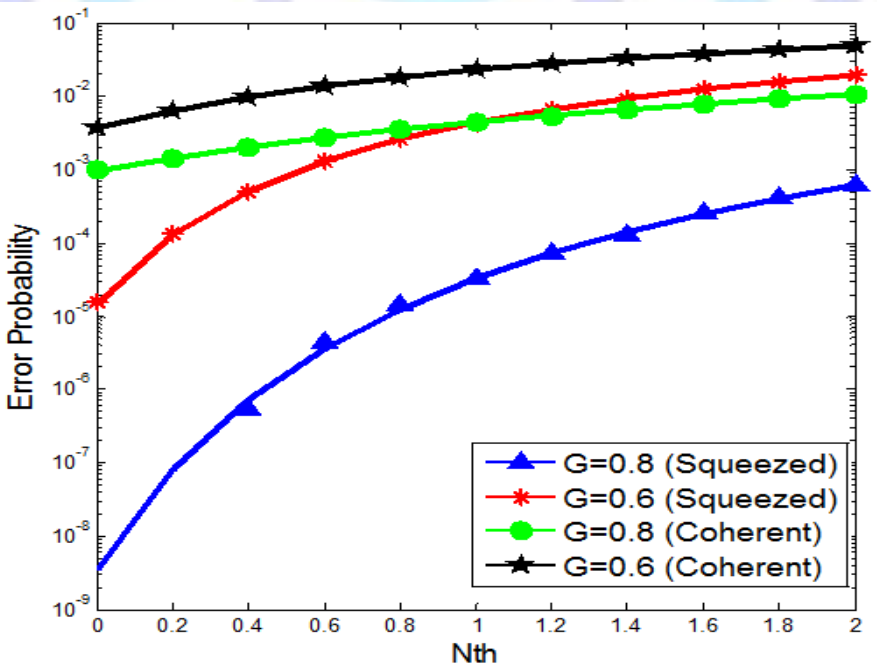

Figure 26: Simulation error probability comparison for $\alpha^2 = 3$ and G=0.6, 0.8 with varying N_{th}. The circles are the simulation results; the solid lines represent the theoretical results.

Figure 26 represents a comparison from thermal noise point of view with $\alpha^2 = 3$ and for two values of G, 0.6 and 0.8. It is found that the error probabilities for a dissipation of 0.8 are 2×10^{-3} and $8 \times 10^{-7}$for the coherent state and the squeezed state, respectively. The squeezed state is better than the coherent state by about four order of magnitude, t. Even a

squeezed state with high dissipation of G=0.6 gives less error probability compared with a coherent state with less dissipation G=0.8. Furthermore, the error probabilities for the squeezed state at G=0.6 and the coherent state at G=0.8 have the following important notes

(i) From N_{th}=0 to 1, the error due to the squeezing dominates because N_{th} is low and the number of photons is higher than that of the coherent state. On the other hand the ratio $\left(\sqrt{NG}/\sqrt{2}\sigma\right)_{sq} > \left(\sqrt{NG}/\sqrt{2}\sigma\right)_{coh}$. Thus, $P_{e,sq} < P_{e,coh}$.

(ii) At N_{th}=1, $\left(\sqrt{NG}/\sqrt{2}\sigma\right)_{sq} = \left(\sqrt{NG}/\sqrt{2}\sigma\right)_{coh}$. Hence the two error probabilities are equal $P_{e,sq} = P_{e,coh}$.

(iii) For $N_{th} > 1$, $\left(\sqrt{NG}/\sqrt{2}\sigma\right)_{sq} < \left(\sqrt{NG}/\sqrt{2}\sigma\right)_{coh}$. Therefore, $P_{e,sq} > P_{e,coh}$.

(iv) Thus, there is a trade-off between the number of photons and the dissipation when N_{th} increases to get the same value of P_e.

3 CONCLUSIONS

The following concluding remarks are drawn from the experimental and computational investigations:

1. Experimentally, it is convenient to choose the He-Ne laser to generate the quantum squeezed states because it offers low noise, high power stability, and long life operation. Moreover, it is very easy to calibrate the light between the two arms of the interferometer due the visibility and the safety of the laser.
2. The homodyne receiver offers an excellent detection because it is successfully able to discriminate between the incoming states. This can be seen by the error probability curves which demonstrate a perfect matching between theoretically and experimentally results.
3. The squeezed state is less sensitive to the environment noise and to the dissipation during transmission as compared with coherent state.
4. The preliminary calculations to design the squeezed light using OPO gives the regularities and the requirements of specific devices to generate such state. The first and the second harmonics are successfully generated using an Nd-YAG laser. The required powers are sufficient to generate the beat the nonlinear crystal inside the squeezed cavity.
5. Pound-Drever-Hall technique is successfully implemented to stabilize the squeezed cavity.
6. The maximum obtained squeezing is -6.30 dB below the quantum noise limit which is sufficient to be implemented in quantum communication to enhance system performance of coherent state counterpart.
7. The error probability of binary communication system employing squeezed state is better than the coherent state by about four order of magnitude. Even a squeezed state with high dissipation of G=0.6 gives less error probability compared with a coherent state with less dissipation G=0.8.

ACKNOWLEGMENT

Great thanks are gone to the *Applied Quantum Mechanics Group* in the University of Milano, Italy, especially *Prof. Matteo G. A. Paris, Dr. Simone Cialdi, Prof. Fabrizio Catelli and Dr. Stefano Olivares,* for their genuine assistant in carrying out the experimental work.

Author' biography

Ismael Shanan Desher was born in Baghdad, Iraq, in 1965. He received the MSc degree in Electrical Engineering from the University of Baghdad, Iraq, in 2007. He joined the staff of the Department of Electrical Engineering, University of Baghdad, as assistant lecturer in 2007. Currently he is working toward the PhD degree in Electronic and Communications engineering at the Institute of Laser for Postgraduate Studies, University of Baghdad. His research interests include quantum communication.

Raad Sami Fyath was born in Maysan, Iraq, in 1954. He received the BSc degree in electrical engineering from the University of Basra, Iraq, in 1976 , the MSc degree in electronics and communications engineering from the University of Baghdad, Iraq, in 1987, and the PhD degree in electronics Engineering from University of Wales-Bangor, UK, in 1990. Currently, he is a professor of electronics and communications engineering at the College of Engineering, Alnahrain University, Baghdad, Iraq. His research interests include optical and wireless communications, Optoelectronics, and Nanophotonics. He published more than 100 papers in different scientific journals and conference proceedings.